Ions Generated from Uranyl Nitrate Solutions by Electrospray Ionization (ESI) and Detected with Fourier Transform Ion-Cyclotron Resonance (FT-ICR) Mass Spectrometry

Sofie Pasilis,* Árpád Somogyi, Kristin Herrmann, and Jeanne E. Pemberton
Department of Chemistry, University of Arizona, Tucson, Arizona, USA

Electrospray ionization (ESI) of uranyl nitrate solutions generates a wide variety of positively and negatively charged ions, including complex adducts of uranyl ions with methoxy, hydroxy, and nitrate ligands. In the positive ion mode, ions detected by Fourier transform ion cyclotron resonance (FT-ICR) mass spectrometry are sensitive to instrumental tuning parameters such as quadrupole operating frequency and trapping time. Positive ions correspond to oligomeric uranyl nitrate species that can be characterized as having a general formula of $[(UO_2)_n(A)_m(CH_3OH)_s]^+$ or $[(UO_2)_n(O)(A)_m(CH_3OH)_s]^+$ with n = 1–4, m = 1–7, s = 0 or 1, and A = OH, NO_3, CH_3O or a combination of these, although the formation of NO_3-containing species is preferred. In the negative ion mode, complexes of the form $[(UO_2)(NO_3)_m]^-$ (m = 1–3) are detected, although the formation of the oxo-containing ions $[(UO_2)(O)_n(NO_3)_m]^-$ (n = 1–2, m = 1–2) and the hydroxy-containing ions $[(UO_2)(OH)_n(NO_3)_m]^-$ (n = 1–2, m = 0–1) are also observed. The extent of coordinative unsaturation of both positive and negative ions can be determined by ligand association/exchange and H/D exchange experiments using D_2O and CD_3OD as neutral reaction partners in the gas-phase. Positive ions are of varying stability and reactivity and may fragment extensively upon collision with D_2O, CD_3OD and N_2 in sustained off-resonance irradiation/collision-induced dissociation (SORI-CID) experiments. Electron-transfer reactions, presumably occurring during electrospray ionization but also in SORI-CID, can result in reduction of U(VI) to U(V) and perhaps even U(IV). (J Am Soc Mass Spectrom 2006, 17, 230–240) © 2006 American Society for Mass Spectrometry

The aqueous chemistry of uranium influences important technological, biological, and geochemical processes involving this element, including its mobility and fate in the geologic subsurface, bioavailability and carcinogenicity, the genesis of uranium mineral deposits and uranium mining, nuclear fuel reprocessing, and the migration of nuclear wastes. However, while great strides have been made in understanding uranium speciation in aqueous systems and the thermodynamic properties of organic and inorganic uranium complexes, the complexity of uranium chemistry sustains existing confusion regarding the existence of individual species under particular conditions of pH, temperature, ionic strength, solution concentration of uranium, and potential complexing ligands. One major difficulty is the paucity of methods that can be used to distinguish specific molecular species at low concentration in solution. Electrospray ionization mass spectrometry (ESI-MS) can provide molecular weight and structural information and has been used successfully for molecular characterization of U(VI) complexes with ligands of environmental or biological interest [1–5]. However, much fundamental work on the complex gas-phase chemistry of U(VI) and U(VI)-containing species remains to be done before ESI-MS can be used to characterize U(VI) species in natural waters.

Previous studies on the gas-phase reactivity of uranium ions have been reported. Many of these studies have focused on the reactions of U^+ and UO^+ with alkanes [6, 7], alkenes [8], alcohols, thiols and ethers [9], arenes [10], and other small molecules [11–16]. Recently, the hydration reactivities of UO^+, UO_2^+, and UO_2^{2+} were examined using secondary ion mass spectrometry [17]. These studies used surface ionization [11, 12], pulsed glow discharge [13, 14], or laser ablation [6–11, 13, 16, 17] techniques to create uranium ions for study. In addition, several studies have used electrospray ionization combined with an ion trap instrument to generate various UO_2^{2+}-ligand complexes from solu-

Published online January 18, 2006

Address reprint requests to Dr. J. E. Pemberton, Department of Chemistry, University of Arizona, 1306 East University Blvd., Tucson, AZ 85721, USA.E-mail: pembertn@u.arizona.edu

* Current address: Chemical Sciences Division, Oak Ridge National Laboratory, Oak Ridge, TN 37831.

1044-0305/06/$32.00
doi:10.1016/j.jasms.2005.10.015

Received July 29, 2005
Revised October 26, 2005
Accepted October 26, 2005

tion and study their gas-phase reactivity with neutral solvent molecules [18–21].

In the present study, we use Fourier transform ion cyclotron resonance (FT-ICR) mass spectrometry to elucidate the gas-phase behavior of uranyl-containing species. To the best of our knowledge, this is the first systematic investigation using FT-ICR mass spectrometry to obtain accurate mass measurements on gas-phase uranyl-containing ions, as well as to examine ligand association/exchange and H/D exchange reactions of these species.

Experimental

Uranyl nitrate hexahydrate, $UO_2(NO_3)_2 \cdot 6\ H_2O$ (J. T. Baker) was received as a gift from the University of Arizona Radiation Control Office and recrystallized before use. Water (18 MΩ, total organic carbon <10 ppb) was purified with a Milli-Q UV system (Millipore Corporation, Billerica, MA). D_2O (99.9% D) and CD_3OD (99.8% D) were purchased from Cambridge Isotopes (Andover, MA) and were introduced into the ICR cell through a leak valve after several steps of degassing.

Samples were prepared from a 1 mM stock solution of uranyl nitrate in H_2O. Samples for FT-ICR MS measurements were prepared by diluting the stock solution with methanol. Solutions from which positive ion spectra were acquired were 330 μM in UO_2^{2+} and 660 μM in NO_3^- in a 66% CH_3OH/33% H_2O (vol/vol) solvent system; solutions from which negative ion spectra were acquired were 50 μM in UO_2^{2+} and 100 μM in NO_3^- in a 95% CH_3OH/5% H_2O (vol/vol) solvent system.

An IonSpec 4.7 T Fourier ion cyclotron resonance (FT-ICR) instrument (Lake Forest, CA) was used for ultrahigh resolution/accurate mass measurements, as well as for gas-phase ligand association/exchange and H/D exchange studies. Ions were generated using an Analytica (Branford, CT) second-generation electrospray source. Ions were introduced into the instrument by infusing sample solutions using a stainless steel microelectrospray needle (0.10 mm i.d.) at a flow rate of 2 μL/min. The capillary temperature was kept at 60 °C. For positively charged ions, a needle voltage of 3.8 kV was applied, while −2.5 kV was used in the negative ion mode. Once generated, the ions pass through a skimmer that retards the passage of neutral molecules and restricts the pressure, and then are accumulated in an external RF-only hexapole for 400–1000 ms. The accumulated ions are passed through the high-speed shutter into the RF-only quadrupole ion guide where they are focused and guided into the ICR cell where they are trapped. The quadrupole ion guide acts as a mass filter and has two operating frequencies, 1820 and 965 kHz. According to the manufacturer, these two frequencies allow trapping of ions in the ranges of *m/z* 100–1000 and *m/z* 400–2500, respectively.

This instrument was modified in-house to accommodate ligand association/exchange and H/D exchange reactions by incorporating the pulsed-leak configuration described by Jiao et al. [22]. Typical analyzer base pressures are 7×10^{-11} torr. The pulsed-leak configuration allows introduction of reagent gas into the analyzer region at a constant partial pressure for a specified period of time.

The ion gauge used to determine reagent gas pressures was calibrated using betaine, which contains one exchangeable proton with a known exchange rate constant [23]. The partial pressures of D_2O and CD_3OD exchange reagents were corrected for ion gauge sensitivities [24]. The corrected, calibrated pressure of D_2O gas used for these experiments was $(2.4 \pm 0.5) \times 10^{-8}$ torr, while the corrected, calibrated pressure of CD_3OD gas was $(4.8 \pm 0.3) \times 10^{-8}$ torr. Ion-molecule reaction times were varied from 10 to 180 s. For H/D and ligand exchange experiments, all trapped ions except those of interest are ejected from the ICR cell via a chirp frequency sweep. The isolated ions are allowed to cool for several seconds before the reagent gas is leaked into the analyzer region. At the end of a specified reaction time under constant exchange reagent pressure, neutral reagent gas was pumped away during a 30 s pump-down to reach the very low pressures necessary for FT-ICR analysis. Pressure in the ICR cell at the time of detection was $\sim 3.5 \times 10^{-9}$ torr.

Various spectral calibration procedures were used to obtain exact mass values. For positively-charged uranyl nitrate-containing species of *m/z* >900, a peak matching procedure using Ultramark 1621 (Lancaster Synthesis, Inc., Lancashire, UK) was used. For positive species of lower mass, ions previously reported were used for self-internal calibration. For MS/MS and D_2O/CD_3OD ion-molecule reaction spectra, ions previously assigned using Ultramark 1621 were used whenever possible for self-internal calibration. For negative ions, linear alkylbenzene sulfonates (LAS) were initially used for internal calibration and to verify ion assignments. For subsequent studies, unambiguously-assigned uranyl-containing ions were used for self-internal calibration. Ions used for calibration are marked with an asterisk in the tables.

Results and Discussion

Influence of Tuning Parameters on ESI Mass Spectra

Electrospray ionization of uranyl nitrate solutions generates a wide variety of positively charged uranyl-containing ions. These species include not only the relatively simple $[(UO_2)(A)S_n]^+$ ions, where A is CH_3O, OH, or NO_3 and S is either CH_3OH or H_2O as described in Van Stipdonk et al. [18, 20, 21] and in Chien et al. [19], but also more complex positively charged oligomeric species at higher *m/z*, as well as a number of simple, nitrate-containing, negatively-charged species.

In the positive ion mode, the types of uranyl-containing ions detected using FT-ICR are dependent on such

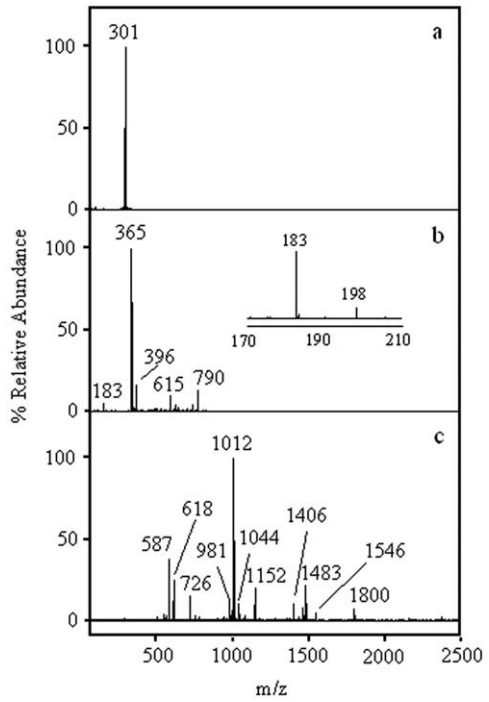

Figure 1. Ions resulting from a solution 330 μM in UO_2^{2+} and 660 μM in NO_3^- in a 66% CH_3OH/33% H_2O (vol/vol) solvent system to indicate the influence of quadrupole trapping frequency, pulse length, and hexapole trapping time on ions in positive ion mass spectra. (**a**) 1820 kHz, 2.881 ms, 1000 ms, (**b**) 965 kHz, 3.167 ms, 400 ms, (**c**) 965 kHz, 3.800 ms, 1000 ms.

instrumental tuning parameters as hexapole trapping time, quadrupole trapping time, and operating frequency, while negative ion spectra are relatively unaffected by changes in these parameters. The different response to instrumental tuning parameters is most likely attributable to the different spray and solvent conditions used for experiments in the positive and negative ion modes. The dependence of ions detected in the positive ion mode on tuning conditions is illustrated in Figure 1a, b, and c. These ESI-MS spectra were acquired under three different ion accumulation conditions, but identical electrospray conditions. Measured and calculated masses of the most abundant ions observed in Figure 1a, b, and c are given in Table 1. Although the measurements discussed in this paper cannot provide direct evidence for the structures of these ions since only chemical composition can be determined by accurate mass measurement, structural features such as those shown in Table 1 and throughout this report are suggested to aid the reader's understanding. It should be noted in this regard that certain structures could involve different atom oxidation states. Since based on *m/z* values alone, charge state assignment for individual moieties cannot be made unambiguously, the convention used throughout this work is not to show charges on individual moieties in the complexes, as suggested and applied by Van Stipdonk et al. [21]. Thus, in this format, ions in which different uranyl oxidation states could be present are treated as equivalent.

Use of the higher quadrupole operating frequency (1820 kHz), a relatively short quadrupole trapping pulse length of 2.881 ms, and a hexapole trapping time of 1000 ms results in the detection of $[(UO_2)(CH_3O)]^+$ at *m/z* 301 (Figure 1a). The use of a lower operating frequency (965 kHz) with a longer quadrupole trapping pulse length (3.167 ms) results in the detection of more complex adducts (Figure 1b). Here, a hexapole trapping time of 400 ms was used together with a two-step filament trapping in which the plate potential was first decreased from 10 to 4 V and then to 0 V. The detected species include $[(UO_2)(CH_3O)(CH_3OH)_2]^+$ and $[(UO_2)(NO_3)(CH_3OH)_2]^+$ at *m/z* 365 and *m/z* 396, respectively (Table 1). These ions have been previously characterized by Van Stipdonk et al. [18] in an ion trap mass spectrometer. The inset of Figure 1b shows doubly-charged species corresponding to the radical-containing ions of $[(UO_2)(CH_3O)(CH_3OH)_2]^{2+\cdot}$ (*m/z* 182.5579, Table 1) and $[(UO_2)(NO_3)(CH_3OH)_2]^{2+\cdot}$ (*m/z* 198). The highest mass ion in Figure 1b appears at *m/z* 790 and can be assigned as $[(UO_2)_2(NO_3)_3(CH_3OH)_2]^+$. A related species, $[(UO_2)_2(NO_3)_3(H_2O)_2]^+$, has been detected by Van Stipdonk et al. [18]. Still more complex species were detected with the use of the lower frequency coil (965 kHz), a significantly longer quadrupole trapping pulse length of 3.800 ms, and a hexapole trapping time of 1000 ms (Figure 1c). In this case, only ions of *m/z* >500 appear in the spectrum. Ions with higher mass (>700 Da) correspond to oligomeric uranyl nitrate species that can be characterized as having a general formula of $[(UO_2)_n(A)_m(CH_3OH)_s]^+$ or $[(UO_2)_n(O)(A)_m(CH_3OH)_s]^+$ with n = 2–4, m = 1–7, and s = 0 or 1. In both cases, A can be OH, NO_3, CH_3O or a combination of these, although the formation of nitrate-containing species is clearly preferred (Table 1 for details).

The use of different tuning parameters is obviously important in gaining a more detailed understanding of the formation of gas-phase uranyl species during electrospray ionization. It is difficult to say whether the spectral sensitivity to tuning parameters is (1) due exclusively to possible ion-molecule reactions during the hexapole trapping time, or (2) related to the different hexapole/quadrupole transmittance of ions originally formed in the ESI process. (Note that external ESI source parameters were not changed during these measurements, i.e., the same spray was used, and that the spectra obtained by different tuning parameters were remarkably reproducible.) In any case, the variety of ions detected clearly indicates that the doubly charged UO_2^{2+} participates in rich reaction chemistry during the ESI process, forming numerous chemically- and structurally-distinct species. Given the lack of available information on the solvation of UO_2^{2+} in dilute solutions containing high concentrations of alcohols, it is difficult to say whether any of the detected ions are actual solution-phase species or if they are simply formed during the electrospray process.

Table 1. Assignments for positive ions resulting from a solution 330 μM in UO_2^{2+} and 660 μM in NO_3^- in a 66% CH_3OH/33% H_2O (vol/vol) solvent system

Nominal *m/z*[a]	Observed *m/z*	Calculated *m/z*	Assignment
301	301.0590	301.0590	$[(UO_2)(CH_3O)]^+$
183	182.5579	182.5557	$[(UO_2)(CH_3O)(CH_3OH)_2]^{2+\cdot}$
198	198.0424	198.0404	$[(UO_2)(NO_3)(CH_3OH)_2]^{2+\cdot}$
365*	365.1114	365.1114	$[(UO_2)(CH_3O)(CH_3OH)_2]^+$
396	396.0797	396.0809	$[(UO_2)(NO_3)(CH_3OH)_2]^+$
790	790.1009	790.0971	$[(UO_2)_2(NO_3)_3(CH_3OH)_2]^+$
572*	572.0711	572.0711	$[(UO_2)_2(O)_2]^+$
587	587.0949	587.0945	$[(UO_2)_2(O)(CH_3O)]^+$
615			unassigned
618	618.0639	618.0640	$[(UO_2)_2(O)(NO_3)]^+$
726	726.0465	726.0447	$[(UO_2)_2(NO_3)_3]^+$
981	981.1155	981.1108	$[(UO_2)_3(O)(NO_3)_2(CH_3O)]^+$
1012	1012.0760	1012.0802	$[(UO_2)_3(O)(NO_3)_3]^+$
1044	1044.1065	1044.1064	$[(UO_2)_3(O)(NO_3)_3(CH_3OH)]^+$
1152	1152.0856	1152.0871	$[(UO_2)_3(NO_3)_5(CH_3OH)]^+$
1406	1406.0990	1406.0964	$[(UO_2)_4(O)(NO_3)_5]^+$
1469	1469.0967	1469.0921	$[(UO_2)_4(NO_3)_6(OH)]^+$
1483	1483.1106	1483.1077	$[(UO_2)_4(NO_3)_6(CH_3O)]^+$
1546	1546.1078	1546.1034	$[(UO_2)_4(NO_3)_7(CH_3OH)]^+$
1800	1800.0585		unassigned

[a] *m/z* Species denoted with * indicate ions used for calibration; ions of *m/z* >900 were calibrated using Ultramark 1621.

Table 2. Assignments for positive ions resulting from reaction of D_2O with high-mass positive ions at selected *m/z*

Nominal *m/z*[ab]	Observed *m/z*	Calculated *m/z*	Assignment
1483*	**1483.1077**	**1483.1077**	**$[(UO_2)_4(NO_3)_6(CH_3O)]^+$**
1502	1502.1260	1502.1246	$[(UO_2)_4(NO_3)_6(CH_3O)(HOD)]^+$
1503	1503.1322	1503.1309	$[(UO_2)_4(NO_3)_6(CH_3O)(D_2O)]^+$
1519	1519.1600	1519.1592	$[(UO_2)_4(NO_3)_6(CH_3O)(CD_3OD)]^+$
1012	**Not obs.**	**1012.0802**	**$[(UO_2)_3(O)(NO_3)_3]^+$**
1051	1051.1227	1051.1202	$[(UO_2)_3(O)(NO_3)_3(D_2O)(HOD)]^+$
1052	1052.1268	1052.1264	$[(UO_2)_3(O)(NO_3)_3(D_2O)_2]^+$
1068	1068.1597	1068.1546	$[(UO_2)_3(O)(NO_3)_3(D_2O)(CD_3OD)]^+$
1069	1069.1322	1069.1307	$[(UO_2)_3(O)(NO_3)_3(HOD)_3]^+$
1070	1070.1365	1070.1370	$[(UO_2)_3(O)(NO_3)_3(D_2O)(HOD)_2]^+$
1071	1071.1410	1071.1433	$[(UO_2)_3(O)(NO_3)_3(D_2O)_2(HOD)]^+$
1072*	1072.1496	1072.1496	$[(UO_2)_3(O)(NO_3)_3(D_2O)_3]^+$
1086	1086.1672	1086.1652	$[(UO_2)_3(O)(NO_3)_3(D_2O)(HOD)(CD_3OH)]^+$
1087	1087.1720	1087.1715	$[(UO_2)_3(O)(NO_3)_3(D_2O)_2(CD_3OH)]^+$
1088	1088.1800	1088.1778	$[(UO_2)_3(O)(NO_3)_3(D_2O)_2(CD_3OD)]^+$
1103	1103.2029	1103.1997	$[(UO_2)_3(O)(NO_3)_3(D_2O)(CD_3OD)(CD_3OH)]^+$
1104	1104.2091	1104.2060	$[(UO_2)_3(O)(NO_3)_3(D_2O)(CD_3OD)_2]^+$
618*	**618.0640**	**618.0640**	**$[(UO_2)_2(O)(NO_3)]^+$**
637	637.0816	637.0808	$[(UO_2)_2(O)(NO_3)(HOD)]^+$
638	638.0874	638.0871	$[(UO_2)_2(O)(NO_3)(D_2O)]^+$
654	654.1172	654.1153	$[(UO_2)_2(O)(NO_3)(CD_3OD)]^+$
656	656.0974	656.0976	$[(UO_2)_2(O)(NO_3)(HOD)_2]^+$
657	657.1031	657.1039	$[(UO_2)_2(O)(NO_3)(D_2O)(HOD)]^+$
658	658.1086	658.1102	$[(UO_2)_2(O)(NO_3)(D_2O)_2]^+$
676	676.1218	676.1208	$[(UO_2)_2(O)(NO_3)(D_2O)(HOD)_2]^+$
677	677.1289	677.1270	$[(UO_2)_2(O)(NO_3)(D_2O)_2(HOD)]^+$
678	678.1347	678.1333	$[(UO_2)_2(O)(NO_3)(D_2O)_3]^+$
693	693.1543	693.1552	$[(UO_2)_2(O)(NO_3)(D_2O)_2(CD_3OH)]^+$
694	694.1596	694.1615	$[(UO_2)_2(O)(NO_3)(D_2O)_2(CD_3OD)]^+$
574	574.0835	574.0852	$[(UO_2)_2(O)(OD)]^+$
587*	**587.0945**	**587.0945**	**$[(UO_2)_2(O)(CH_3O)]^+$**
590	590.1139	590.1164	$[(UO)_2(OH)(CH_3OD)]^+$
606	606.1105	606.1114	$[(UO_2)_2(O)(CH_3O)(HOD)]^+$
607	607.1165	607.1176	$[(UO_2)_2(O)(CH_3O)(D_2O)]^+$
610	610.1368	610.1396	$[(UO_2)_2(OH)(CH_3OD)(D_2O)]^+$
626	626.1324	626.1345	$[(UO_2)_2(O)(CH_3O)(D_2O)(HOD)]^+$
627	627.1383	627.1408	$[(UO_2)_2(O)(CH_3O)(D_2O)_2]^+$

[a] Reacted ions in bold.
[b] *m/z* Species denoted with * indicate ions used for calibration.

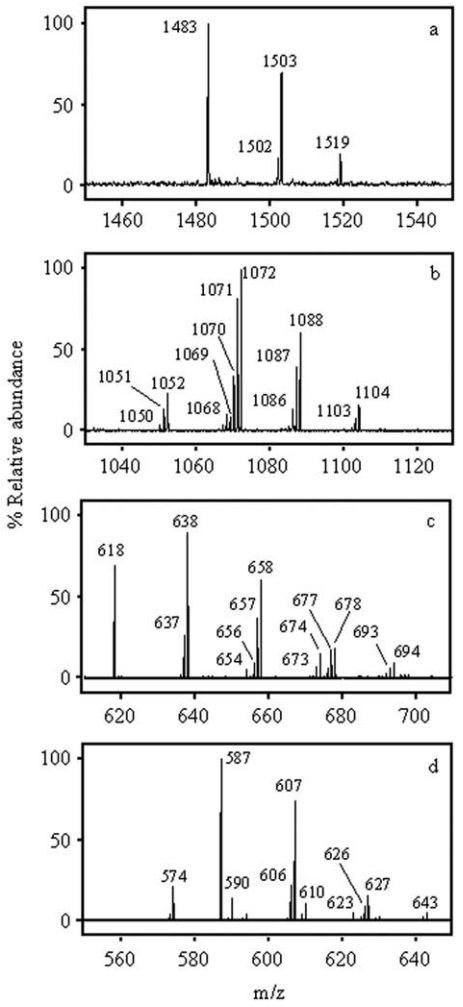

Figure 2. Ions produced by ion-molecule reactions between D_2O and high-mass positive ions at (**a**) *m/z* 1483, (**b**) *m/z* 1012, (**c**) *m/z* 618, and (**d**) *m/z* 587. Reaction time was 10 s in each case with a D_2O pressure of 2.4×10^{-8} torr.

The MS/MS fragmentation patterns of the low mass species (<500 Da) in Figure 1a and b have been previously discussed [18]. The fragmentation patterns of the higher mass species shown in Figure 1c are discussed below.

Ion-Molecule Reactions in the Gas-Phase with D_2O and CD_3OD as Reaction Partners

Ion-molecule reactions in the gas-phase have been used extensively to gain information on the chemistry and reactivity of metals in coordination complexes, as well as the structures of these metal-ligand complexes [25–34]. In our studies, D_2O and adventitious CD_3OD were used as neutral reaction partners with several of the more abundant ions in Figure 1c to assess the degree of coordinative unsaturation of the uranyl in each of the selected species. Representative spectra of the reaction region obtained after reaction of the major ions in Figure 1c with D_2O for 10 s at 2.4×10^{-8} torr are shown in Figure 2a, b, c, and d. Introduction of D_2O into the FT-ICR cell results not only in reaction products but also in some fragmentation of the selected ion. As an example, a representative full-scale spectrum of products appearing upon reaction of $[(UO_2)_3(O)(NO_3)_3]^+$ (*m/z* 1012) with D_2O is shown in Figure 3. Assignments and exact mass values for the ions shown in Figure 2a, b, c, and d and Figure 3 are provided in Table 2.

Upon examination of the spectra in Figure 2a, b, c, and d and the data in Table 2, two patterns emerge. First, the selected ion may undergo a simple addition of one or more D_2O ligands, and the number of D_2O ligands accepted appears to depend on the structure of the ion. H_2O and HOD additions also occur, indicating the presence of residual H_2O in the FT-ICR cell that participates in H/D exchange reactions with D_2O. Additions of CD_3OD are also apparent and must result from residual CD_3OD in the analyzer region of the system or the exchange reagent reservoir/pulsed leak system.

The highest mass ion selected, $[(UO_2)_4(NO_3)_6(CH_3O)]^+$ at *m/z* 1483, undergoes only a simple single addition of HOD, D_2O, or CD_3OD, forming ions at *m/z* 1502, 1503, and 1519, respectively (Figure 2a). These products are also the only ones formed after a 60 s D_2O reaction time (data not shown). Although based on these data alone the structure of this ion cannot be definitely determined, its lack of reactivity is one indication that the uranyl centers are as fully coordinatively saturated as possible except for one site; therefore, the ion is unable to accept more than one ligand at this pressure. Although the full spectrum is not shown here, an ion at *m/z* 270 also appears in the spectrum. This ion corresponds to UO_2^+, and it is observed in the fragmentation spectra of other positively charged uranyl-containing species as well. The intensity of this ion is an indicator of the extent of ion fragmentation that must be related to the stability of a given uranyl complex. Upon reaction of $[(UO_2)_4(NO_3)_6(CH_3O)]^+$ (*m/z* 1483) with D_2O, the UO_2^+ peak is small, indicating that the ion is relatively stable and does not fragment extensively. Presumably, the four UO_2^{2+} groups are coordinatively saturated by nitrate in an oligomeric structure, although it is difficult to predict the structure of this ion based only on its presence and stability.

Another "nonreactive" ion is $[(UO_2)_3(NO_3)_5(CH_3OH)]^+$ at *m/z* 1152. This ion apparently fragments on collision with D_2O, but does not add a D_2O ligand, indicating again that all coordination sites are filled (spectrum not shown).

$[(UO_2)_3(O)(NO_3)_3]^+$ at *m/z* 1012 is significantly more reactive than $[(UO_2)_4(NO_3)_6(CH_3O)]^+$ and undergoes addition of up to three more ligands (Figure 2b, Table 2). After a D_2O reaction time of 10 s, the parent ion has completely disappeared. The greater reactivity of this ion at this pressure is an indication that the uranyl groups in $[(UO_2)_3(O)(NO_3)_3]^+$ are coordinatively less saturated than those in $[(UO_2)_4(NO_3)_6(CH_3O)]^+$ (*m/z*

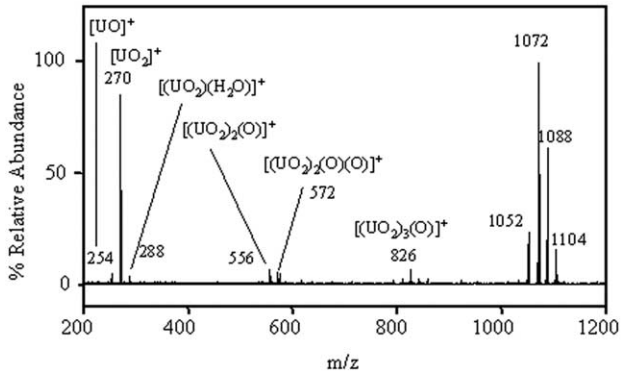

Figure 3. Representative mass spectrum showing fragmentation of *m/z* 1012 and its reaction products after 10 s reaction with D_2O (2.4×10^{-8} torr).

1483), and implies structural differences between the two ions. $[(UO_2)_3(O)(NO_3)_3]^+$ contains what may be a bridging oxygen ligand between the three uranyl groups. The addition of three D_2O or CD_3OD ligands suggests that each uranyl moiety can accommodate only one more ligand in addition to the nitrates, which probably have bidentate coordination to the uranyl. $[(UO_2)_3(O)(NO_3)_3]^+$ also undergoes more extensive fragmentation upon reaction with D_2O (Figure 3) than does $[(UO_2)_4(NO_3)_6(CH_3O)]^+$, which is evidence that it is the more fragile species.

It is interesting to compare the reactions of $[(UO_2)_2(O)(CH_3O)]^+$ at *m/z* 587 and $[(UO_2)_2(O)(NO_3)]^+$ at *m/z* 618 with D_2O, as these ions differ only in whether they contain a methoxy or a nitrate ligand (Figure 2c and d, Table 2). Interestingly, $[(UO_2)_2(O)(NO_3)]^+$ adds three ligands after a 10 s reaction time, while $[(UO_2)_2(O)(CH_3O)]^+$ only accommodates two. DFT calculations indicate that nitrate can coordinate to uranyl in either a bidentate or monodentate configuration in gas-phase $[(UO_2)(NO_3)(H_2O)_3]^+$ complexes [19]. A monodentate bridging nitrate ligand in $[(UO_2)_2(O)(NO_3)]^+$ could, in theory, provide a free nonbridging oxygen atom of the nitrate with which additional D_2O or CD_3OD could interact through hydrogen bonding. Under this scenario, a free oxygen atom is not available for such hydrogen bonding when methoxy replaces nitrate in the complex, and therefore, fewer ligands can be added. Interestingly, $[(UO_2)_2(O)(NO_3)]^+$ fragments less extensively than $[(UO_2)_2(O)(CH_3O)]^+$ upon reaction with D_2O, indicating that it is the more stable ion (spectrum not shown). One other major difference between the two ions is that $[(UO_2)_2(O)(CH_3O)]^+$ undergoes a methoxy/deuteroxy replacement reaction, forming $[(UO_2)_2(O)(OD)]^+$ at *m/z* 574 (Figure 2d). A similar replacement is not seen for $[(UO_2)_2(O)(NO_3)]^+$ consistent with the above contention of its greater stability.

As mentioned above, fragmentation of the selected ions occurs during reaction with D_2O, indicating that these species are fragile. The full-scale spectrum of $[(UO_2)_3(O)(NO_3)_3]^+$ (*m/z* 1012) after reaction with D_2O is shown in Figure 3 as an example. Characteristic ions appearing in all reaction spectra include UO^+ at *m/z* 254, UO_2^+ at *m/z* 270, and $[(UO_2)H_2O]^+$ at *m/z* 288 or $[(UO_2)OH]^+$ at *m/z* 287. $[(UO_2)_2(O)]^+$ and $[(UO_2)_2(O)_2]^+$, which appear at *m/z* 556 and 572, respectively, are also seen in the MS/MS spectra obtained using sustained off-resonance ionization collision-induced dissociation (SORI-CID) with N_2. The ion $[(UO_2)_3(O)]^+$ at *m/z* 826 is unique to the D_2O reaction spectrum of $[(UO_2)_3(O)(NO_3)_3]^+$, and may be evidence for oxygen bridging between three reduced uranyl groups. However, $[(UO_2)_2(O)]^+$, $[(UO_2)_2(O)_2]^+$ and $[(UO_2)_3(O)]^+$ have also been reported from fast atom bombardment studies of inorganic and organic uranyl complexes [35–38], and could result from rearrangements occurring upon fragmentation.

Other ions in Figure 3 are due to formal addition of $D^\cdot$ or exchange of D^+ for H^+ in OH^- to yield OD^-, giving the assignments of $[(UO_2)D]^{+\cdot}$ (*m/z* 272) (not visible in spectrum), $[(UO_2)_2(OD)]^+$ (*m/z* 558), and $[(UO_2)_2(O)(OD)]^+$ (*m/z* 574). The appearance of deuterium in these ions is interesting, since it has been proposed previously that hydrated UO_2^{2+} in solution abstracts a hydrogen atom from water during photolysis, ultimately forming UO_2^+ and H^+ along with an OH radical [39]. A similar solution reaction has been proposed with CH_3OH [39].

Despite the observed differences in stability of these oligomeric uranyl ions, clearly they add ligands only up to the point of coordinative saturation of the uranyl centers at the applied D_2O pressure. Interestingly, as shown by the data in Table 2, for ions containing two, three or four uranyl centers, coordinative saturation is achieved with fewer ligands per uranyl center than observed previously for ions with a single uranyl center [18]. This observation clearly supports the presence of bridging ligands in ions containing multiple uranyl centers that are not possible in ions containing a single uranyl center.

As demonstrated above, most of the selected ions react extensively with D_2O. It is desirable, therefore, to determine how readily the "naked" UO_2^+ singly charged cation (*m/z* 270) reacts with D_2O and CD_3OD in the FT-ICR cell. In both experiments, the ion-molecule reaction times were the same as for *m/z* 301 (180 s) but the pressures were slightly different (2.4×10^{-8} torr for D_2O and 4.8×10^{-8} torr for CD_3OD). UO_2^+ reacts readily with CD_3OD by adding three and four CD_3OD molecules leading to the $[(UO_2)(CH_3OD)_3]^+$ ion at *m/z* 378 and the $[(UO_2)(CH_3OD)_4)]^+$ ion at *m/z* 414 (spectrum not shown). In contrast, no D_2O addition was observed when D_2O was used as a reaction partner. The absence of adducts with D_2O does not necessarily mean that addition reactions do not occur. These adducts could easily fragment under these relatively low-pressure conditions because of the lack of efficient collisional cooling. This explanation is further supported by the observation of $[UO_2(H_2O)_3]^+$ and $[UO_2(H_2O)_4]^+$ in ion trap studies at higher partial pressures of water [17].

Another interesting difference is that doubly-

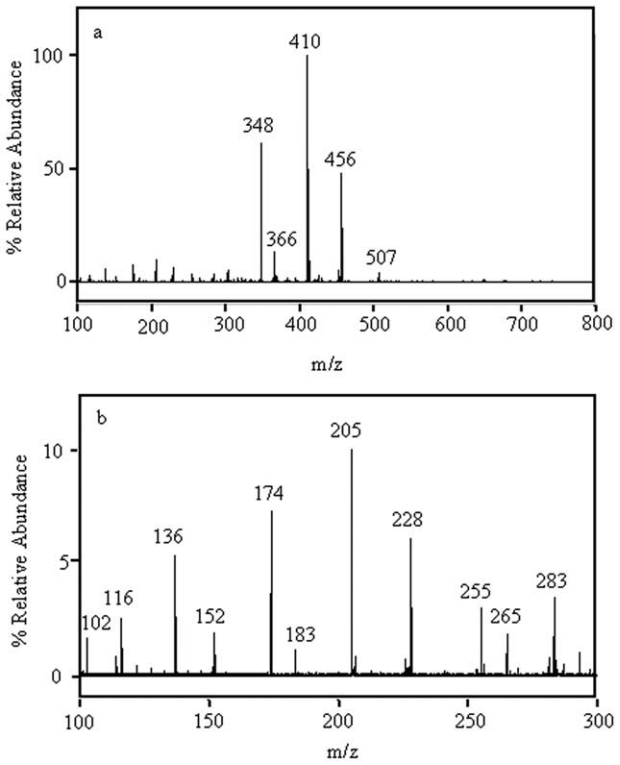

Figure 4. Negative ion ESI mass spectra of a solution containing 50 μM UO_2^{2+} and 100 μM NO_3^- in 95% CH_3OH/5% H_2O (vol/vol). (**a**) Full-scale with singly-charged ions indicated. (**b**) Expanded view of low mass region showing multiply-charged ions.

charged UO_2^{2+} (*m/z* 135) appears in the spectrum after reaction with D_2O, but is absent when CD_3OD is used (spectra not shown). The doubly-charged UO_2^{2+} observed at *m/z* 135 in the presence of D_2O can result from $DO^{\cdot}$ radical addition followed by DO^- anion elimination as suggested earlier [39]. The absence of doubly-charged UO_2^{2+} in the spectrum resulting from reaction with CD_3OD indicates that a similar process does not occur with the methoxy radical.

In addition to conventional methanol adducts, ions associated with the addition of CD_3OCD_3 are also observed. The most prominent of these are the $[(UO_2)(D)(CD_3OD)(CD_3OCD_3)_2]^+$ at *m/z* 412 and the $[(UO_2)(CD_3OD)_2(CD_3OCD_3)_2]^+$ at *m/z* 446. The perdeuterodimethyl ether can form either in the cell at the partial pressure of CD_3OD used for these studies (~4.8×10^{-8} torr) [40, 41] or at the uranyl ("catalytic") centers. A more detailed investigation of the *m/z* 411–414 region also reveals another ion at *m/z* 412 corresponding to $[(UO_2)(CD_3O)(CD_3OD)_3]^+$.

Negative Ions Containing Uranyl and Nitrate Generated by ESI

Alkali and transition-metal cations are known to form complexes with nitrate when an excess of NO_3^- is present in solution [42, 43]. Generally, these complexes are of the form $[(UO_2)(NO_3)_m]^-$ (m = 1–3), although the formation of oxo-nitrate ($[(UO_2)(O)(NO_3)_m]^-$ (m = 1–2) and hydroxy-nitrate ($[(UO_2)(OH)_n(NO_3)_m]^-$ (*n* = 1–2, m = 0–1) products are also observed [43]. In agreement with these previous observations, we have also detected uranyl nitrate and oxo-nitrate gas-phase complexes in the negative ion mode (Figure 4a). An expanded view of the low mass region is shown in Figure 4b. Measured and calculated masses of the ions observed are given in Table 3. These negative ion spectra were acquired using a quadrupole operating frequency of 1820 kHz with a quadrupole trapping pulse length of 3.200 ms. In contrast to the behavior observed with positive ions, changing these ion accumulation parameters did not affect the negative ion species detected.

The three most intense ions in Figure 4a appear at *m/z* 348, 410 and 456. The ion at *m/z* 456 is assigned to $[(UO_2)(NO_3^-)_3]^-$. This gas-phase ion is identical to the solution-based uranyl trinitrate complex, $[(UO_2)^{2+}(NO_3^+)_3]^-$, known to form in ketones, ethers and alcoholic solvents; the stability of the complex decreases in the order ketone > ether > alcohol > water, which indicates a competition between solvent and nitrate for positions in the coordination sphere of UO_2^{2+} in solution [44]. Therefore, complexation by nitrates can easily occur during desolvation, when coordinating solvent molecules are stripped away. In the crystal structure of $Rb[(UO_2)(NO_3)_3]$, each nitrate group chelates uranyl in a bidentate fashion, and the conformation around U(VI) is hexagonal bipyramid [45]. The coordination of $[(UO_2)(NO_3)_3]^-$ in the gas-phase is presumed to be similar.

The ion at *m/z* 410 can be assigned to $[(UO_2)(O)(NO_3)_2]^-$, which is supported by the observation that O^{2-} may undergo oxidation to form O^- in gas-phase metal oxo-complexes [43]. However, note again that based solely on *m/z* determination, the charge states of individual components of these complexes cannot be definitively known. The ion at *m/z* 348 is assigned as $[(UO_2)(O)(NO_3)]^-$. Two ions of lower intensity appear at *m/z* 366 and *m/z* 507. The first may be assigned to $[(UO_2)(OH)_2(NO_3)]^-$, while the second corresponds to $[(UO_2)(NO_3)_2(CF_3COO)]^-$ and is the result of reaction with residual trifluoroacetate contaminant in the ESI source.

The corresponding doubly, triply, and quadruply-charged ions of the singly-charged species described above are seen in the spectrum below *m/z* 250 (Figure 4b, Table 3). If they are not *exclusively* overtones, these ions may contain uranium in the U(VI), U(V), or U(IV) oxidation states as a result of reduction reactions occurring during electrospray ionization in the negative ion mode. The appearance of the ions $[(UO_2)(O)(NO_3)_2]^{4-}$ (*m/z* 102.5), $[(UO_2)(O)(NO_3)]^{3-}$ (*m/z* 116), and $[(UO_2)(NO_3)_3]^{3-}$ (*m/z* 152) is particularly interesting as they may contain uranium in the U(IV) oxidation state and indicate that both one and two electron additions to UO_2^{2+} may occur during electrospray ionization.

Product-ion spectra of the uranyl-nitrate complexes

Table 3. Assignments for negative ions resulting from a solution containing 50 μM UO_2^{2+} and 100 μM NO_3^- in 95% CH_3OH/5% H_2O (vol/vol)

Nominal *m/z*[a]	Observed *m/z*	Calculated *m/z*	Assignment
102.5	102.5040	102.5028	$[(UO_2)(O)(NO_3)_2]^{4-}$
116	116.0081	116.0078	$[(UO_2)(O)(NO_3)]^{3-}$
136.6	136.6734	136.6704	$[(UO_2)(O)(NO_3)_2]^{3-}$
152	152.0017	152.0014	$[(UO_2)(NO_3)_3]^{3-}$
174	174.0105	174.0117	$[(UO_2)(O)(NO_3)]^{2-}$
183	183.0163	183.0169	$[(UO_2)(OH)_2(NO_3)]^{2-}$
205*	205.0056	205.0056	$[(UO_2)(O)(NO_3)_2]^{2-}$
228	228.0004	228.0020	$[(UO_2)(NO_3)_3]^{2-}$
255	255.2316		
265	265.1469		
283	283.2633		
293	293.1783		
302	302.0301	302.0304	$[(UO_2)(O)_2]^-$
303	303.0379	303.0383	$[(UO_2)(O)(OH)]^-$
304	304.0445	304.0461	$[(UO_2)(OH)_2]^-$
317	317.0538	317.0539	$[(UO_2)(O)(CH_3O)]^-$
321	321.0043		
348	348.0217	348.0233	$[(UO_2)(O)(NO_3)]^-$
364	364.0185	364.0183	$[(UO_2)(O)_2(NO_3)]^-$
366	366.0340	366.0339	$[(UO_2)(OH)_2(NO_3)]^-$
367	367.0222		
367	367.0401	367.0417	$[(UO_2)(OH)_2(NO_3)(H_2O)]^-$
368	368.0468	368.0465	$[(UO_2)(OD)_2(NO_3)]^-$
368			$[(UO_2)(O)(NO_3)(D_2O)]^-$
382	382.9930		contaminant
394	394.0178		
410*	410.0112	410.0112	$[(UO_2)(O)(NO_3)_2]^-$
411	411.0202		
412	412.0153		
413	413.0150	413.0147	$[(UO_2)(F)(NO_3)_2]^-$
425	425.0361		
428	428.9866		
453	453.0317		
456	456.0022	456.0041	$[(UO_2)(NO_3)_3]^-$
507	507.0042	507.0013	$[(UO_2)(NO_3)_2(CF_3COO)]^-$

[a] *m/z* Species denoted with * indicate ions used for calibration.

obtained using SORI-CID are shown in Figure 5a, b, c, and d. These fragmentation reactions follow a pattern similar to those described for transition-metal nitrate complexes, involving loss of NO_2 and the formation of an oxo-nitrate complex followed by loss of NO_3 and reduction of the metal [43]:

$$\left[\left(UO_2^{2+}\right)\left(NO_3^-\right)_3\right]^-\left(m/z\ 456\right) \rightarrow \left[\left(UO_2^{2+}\right)\left(O^-\right)\left(NO_3^-\right)_2\right]^-\left(m/z\ 410\right) + NO_2 \quad (1)$$

$$\left[\left(UO_2^{2+}\right)\left(O^-\right)\left(NO_3^-\right)_2\right]^-\left(m/z\ 410\right) \rightarrow \left[\left(UO_2^{+}\right)\left(O^-\right)\left(NO_3^-\right)\right]^-\left(m/z\ 348\right) + NO_3 \quad (2)$$

Table 4. Assignments for ions resulting from the reaction of $[(UO_2)(NO_3)_2(CF_3COO)]^-$, $[(UO_2)(OH)_2(NO_3)]^-$ and $[(UO_2)(O)(NO_3)]^-$ with D_2O

Nominal *m/z*[ab]	Observed *m/z*	Calculated *m/z*	Assignment
348	348.0231	348.0233	$[(UO_2)(O)(NO_3)]^-$
368	368.0465	368.0465	$[(UO_2)(OD)_2(NO_3)]^-$
410	410.0111	410.0112	$[(UO_2)(O)(NO_3)_2]^-$
456*	456.0041	456.0041	$[(UO_2)(NO_3)_3]^-$
507	507.0015	507.0013	$[(UO_2)(NO_3)_2(CF_3COO)]^-$
366	366.0326	366.0339	$[(UO_2)(OH)_2(NO_3)]^-$
367	367.0220		
367	367.0393	367.0388	$[(UO_2)(OH)(OD)(NO_3)]^-$
368*	368.0465	368.0465	$[(UO_2)(OD)_2(NO_3)]^-$
384	384.0750	384.0747	$[(UO_2)(O)(NO_3)(CD_3OD)]^-$
410	410.0117	410.0112	$[(UO_2)(O)(NO_3)_2]^-$
456	456.0056	456.0041	$[(UO_2)(NO_3)_3]^-$
348	Not obs.	348.0233	$[(UO_2)(O)(NO_3)]^-$
367	367.0411	367.0388	$[(UO_2)(OH)(OD)(NO_3)]^-$
368*	368.0465	368.0465	$[(UO_2)(O)(NO_3)(D_2O)]^-$
384	384.0763	384.0747	$[(UO_2)(O)(NO_3)(CD_3OD)]^-$

[a] Reacted ions in bold. [b] *m/z* Species denoted with *indicate ions used for calibration.

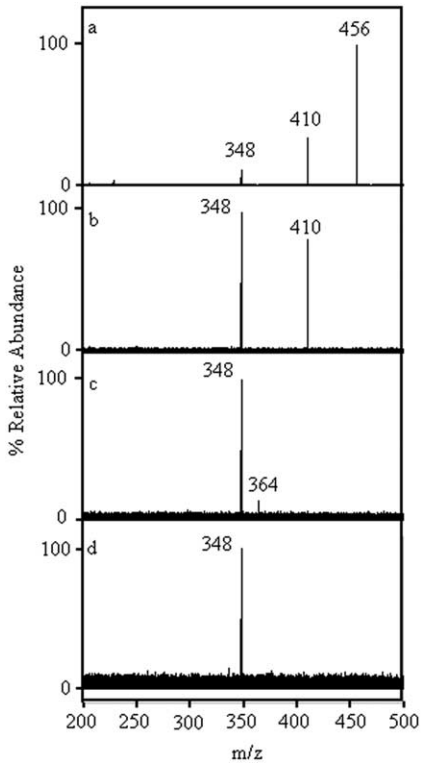

Figure 5. SORI-CID spectra of negatively charged ions at (**a**) *m/z* 456, (**b**) *m/z* 410, (**c**) *m/z* 366, and (**d**) *m/z* 348.

Note that tentative charge states of individual species of the complexes are suggested in eqs 1 and 2 to illustrate possible reduction of the uranyl center. The stable $[(UO_2)(O)(NO_3)]^-$ ion (*m/z* 348) cannot be further fragmented under our SORI-CID conditions. SORI-CID of $[(UO_2)(OH)_2(NO_3)]^-$ (*m/z* 366) results in a simple loss of H_2O, forming $[(UO_2)(O)(NO_3)]^-$ at *m/z* 348. A small peak at *m/z* 364 is attributed to the loss of two hydrogen atoms or H_2 from $[(UO_2)(OH)_2(NO_3)]^-$, with the formation of $[(UO_2)(O)_2(NO_3)]^-$ (Figure 5c).

Ion-Molecule Reactions with Negative Ions Using D_2O

D_2O was used as a neutral reaction partner to compare the reaction chemistry of the anionic uranyl nitrate ions with the chemistry of the positive species discussed above. Representative spectra of the reaction region for the major ions in Figure 4a are collected in Figure 6a, b, c, and d. Assignments and exact mass values are provided in Table 4. All spectra shown in Figure 6a, b, c, and d were obtained through selection and reaction of the ion of interest with D_2O for 180 s at 2.4×10^{-8} torr.

Examination of the spectra in Figure 6a, b, c, and d indicates that the negative uranyl nitrate-containing ions do not undergo the extensive series of reactions upon collision with D_2O as seen for the positively charged uranyl nitrate species (Figure 2a, b, c, d, and Figure 3). With the exception of $[(UO_2)(O)(NO_3)]^-$ at *m/z* 348, D_2O additions are not observed, indicating that these ions are coordinatively saturated.

Neither $[(UO_2)(NO_3)_3]^-$ (*m/z* 456) nor $[(UO_2)(O)(NO_3)_2]^-$ (*m/z* 410) react with D_2O at the pressure used for these experiments (Figure 6a and b). The $[(UO_2)(NO_3)_3]^-$ ion, with its presumed bidentate nitrate groups, is coordinatively saturated and cannot accept a D_2O ligand. $[(UO_2)(O)(NO_3)_2]^-$ most likely has a pentagonal bipyramidal conformation with two bidentate nitrate groups and a single oxygen ligand. Gas-phase uranyl-containing ions with this type of conformation are quite stable [19]. Assuming bidentate coordination by nitrate, $[(UO_2)(OH)_2(NO_3)]^-$ (*m/z* 366) presumably has a conformation in which there is coordination at only four equatorial sites, yet the complex does not accept a D_2O ligand but only undergoes an H/D exchange reaction to form $[(UO_2)(OD)_2(NO_3)]^-$ (*m/z* 368). Only $[(UO_2)(O)(NO_3)]^-$ (*m/z* 348) can accept a D_2O ligand, forming $[(UO_2)(O)(NO_3)(D_2O)]^-$ at *m/z* 368. In both of the latter two cases, a small ion at *m/z* 384 appears as a reaction product. This ion is tentatively assigned to $[(UO_2)(O)(NO_3)(CD_3OD)]^-$ and may result from trace amounts of CD_3OD in the D_2O reagent used for these reactions. Finally, we note that the ions at *m/z* 410, $[(UO_2)(O)(NO_3)_2]^-$ and 456, $[(UO_2)(NO_3)_3]^-$, in Figure 6c, are presumably the result of multiple collision reactions occurring with nitrate-containing species in the FT-ICR cell.

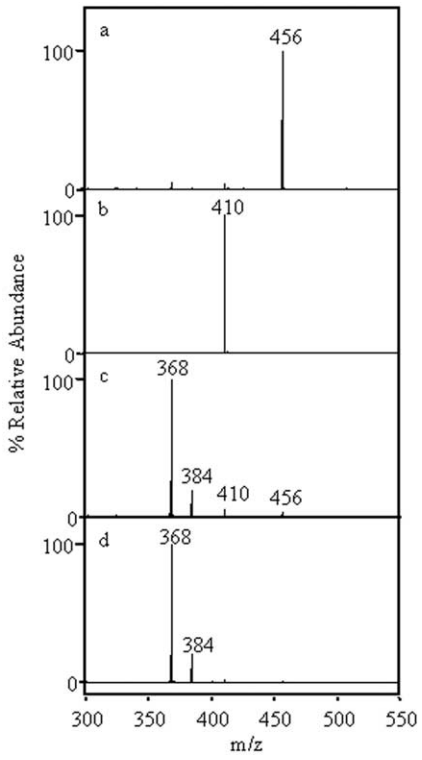

Figure 6. Ions produced by reactions (180 s reaction time) between D_2O (2.4×10^{-8} torr) and negative ions at (**a**) *m/z* 456, (**b**) *m/z* 410, (**c**) *m/z* 366, and (**d**) *m/z* 348.

Conclusions

Electrospray ionization of uranyl nitrate solutions generates a wide variety of positively and negatively charged ions, including complex adducts of uranyl, methoxy, hydroxy, and nitrate ligands, as well as oxygen. In the positive ion mode, the ions detected are highly sensitive to instrumental tuning parameters such as quadrupole operating frequency and trapping time. Ions formed are of varying stability and reactivity with some undergoing extensive fragmentation upon collision with D_2O and others not. The extent of coordinative unsaturation of both positive and negative ions can be investigated using D_2O and CD_3OD as neutral reaction partners within the applied pressure range. Electron-transfer reactions, presumably occurring during electrospray, can result in reduction of U(VI) to U(V) and perhaps even U(IV). SORI-CID fragmentation processes are often coupled with electron-transfer involving both the uranyl moiety and the oxygen ligand, if present.

This simple uranyl nitrate system provides a wealth of both simple and complex ions and illustrates the complexity of the chemical reactions that occur between injection of solution into the ESI source region and analysis in the ICR cell. Most, if not all, of the ions detected were not solution-phase species, but were generated during desolvation or during gas-phase reactions in the instrument. This work demonstrates the utility of FT-ICR, with its ultrahigh resolution and mass accuracy, for the study of the gas-phase reaction chemistry of uranyl and its complexes.

Acknowledgments

The authors gratefully acknowledge support of this research by the National Institutes of Health through the Native American Cancer Research Partnership funded through the Minority Institute Cancer Control Program of the National Cancer Institute (U54CA96281).

References

1. Wu, Q.; Cheng, X.; Hofstadler, S. A.; Smith, R. D. Specific Metal-Oligonucleotide Binding Studied by High Resolution Tandem Mass Spectrometry. *J. Mass Spectrom.* **1996,** *31,* 669–675.
2. Moulin, C.; Charron, N.; Plancque, G.; Virelizier, H. Speciation of Uranium by Electrospray Ionization Mass Spectrometry: Comparison with Time-Resolved Laser-Induced Fluorescence. *Appl. Spectrosc.* **2000,** *54,* 843–848.
3. Jacopin, C.; Sawicki, M.; Plancque, G.; Doizi, D.; Taran, F.; Ansoborlo, E.; Amekraz, B.; Moulin, C. Investigation of the Interaction Between 1-Hydroxyethane-1,1-Diphosphonic Acid (HEDP) and Uranium(VI). *Inorg. Chem.* **2003,** *42,* 5015–5022.
4. Pasilis, S. P.; Pemberton, J. E. Speciation and Coordination Chemistry of Uranyl(VI)-Citrate Complexes in Aqueous Solution. *Inorg. Chem.* **2003,** *42,* 6793–6800.
5. Groenewold, G. S.; Van Stipdonk, M. J.; Gresham, G. L.; Chien, W.; Bulleigh, K.; Howard, A. Collision-Induced Dissociation Tandem Mass Spectrometry of Desferrioxamine Siderophore Complexes from Electrospray Ionization of UO_2^{2+}, Fe^{3+}, and Ca^{2+} Solutions. *J. Mass Spectrom.* **2004,** *39,* 752–761.
6. Heinemann, C.; Cornehl, H. H.; Schwarz, H. Hydrocarbon Activation by "Bare" Uranium Cations: Formation of a Cationic Uranium-Benzene Complex from Three Ethylene Units. *J. Organomet. Chem.* **1995,** *501,* 201–209.
7. Gibson, J. K. Gas-Phase f-Element Organometallic Chemistry: Reactions of Cyclic Hydrocarbons with Th^+, U^+, ThO^+, UO^+, and Lanthanide Ions, Ln^+. *Organometallics* **1997**, *16,* 4214–4222.
8. Gibson, J. K. Gas-Phase Transuranium Organometallic Chemistry: Reactions of Np^+, Pu^+, NpO^+, and PuO^+ with Alkenes. *J. Am. Chem. Soc.* **1998,** *120,* 2633–2640.
9. Gibson, J. K. Gas-Phase Transuranium Chemistry: Reactions of Actinide Ions with Alcohols and Thiols. *J. Mass Spectrom.* **1999,** *34,* 1166–1177.
10. Marcalo, J.; Leal, J. P.; Pires de Matos, A. Gas-Phase Actinide Ion Chemistry: FT-ICR/MS Study of the Reactions of Thorium and Uranium Metal and Oxide Ions with Arenes. *Organometallics* **1997,** *16,* 4581–4588.
11. Armentrout, P. B.; Hodges, R. V.; Beauchamp, J. L. Endothermic Reactions of Uranium Ions with N_2, D_2, and CD_4. *J. Chem. Phys.* **1977,** *66,* 4683–4688.
12. Armentrout, P. B.; Beauchamp, J. L. Reactions of U^+ and UO^+ with O_2, CO, CO_2, COS, CS_2, and D_2O. *Chem. Phys.* **1980,** *50,* 27–36.
13. Cornehl, H. H.; Heinemann, C.; Marcalo, J.; Pires de Matos, A.; Schwarz, H. The "Bare" Uranyl(2+) Ion, UO_2^{2+}. *Angew. Chem. Int. Ed. Engl.* **1996,** *35,* 891–894.
14. Jackson, G. P.; King, F. L.; Goeringer, D. E.; Duckworth, D. C. Gas-Phase Reactions of U^+ and U^{2+} with O_2 and H_2O in a Quadrupole Ion Trap. *J. Phys. Chem. A* **2002,** *106,* 7788–7794.
15. Jackson, G. P.; Gibson, J. K.; Duckworth, D. C. Gas-Phase Reactions of Bare and Ligated Uranium Ions with Sulfur Hexafluoride. *J. Phys. Chem. A* **2004,** *108,* 1042–1051.
16. Gibson, J. K.; Haire, R. G.; Santos, M.; Marcalo, J.; Pires de Matos, A. Oxidation Studies of Dipositive Actinide Ions, An^{2+} (An = Th, U, Np, Pu, Am) in the Gas Phase: Synthesis and Characterization of the Isolated Uranyl, Neptunyl, and Plutonyl Ions UO_2^{2+}(g), NpO_2^{2+}(g), and PuO_2^{2+}(g). *J. Phys. Chem. A* **2005,** *109,* 2768–2781.
17. Gresham, G. L.; Gianotto, A. K.; de Harrington, P.; Cao, L.; Scott, J. R.; Olson, J. E.; Appelhans, A. D.; Van Stipdonk, M. J.; Groenewold, G. S. Gas-Phase Hydration of U(IV), U(V), and U(VI) Dioxo Monocations. *J. Phys. Chem. A* **2003,** *107,* 8530–8538.
18. Van Stipdonk, M.; Anbalagan, V.; Chien, W.; Gresham, G.; Groenewold, G.; Hanna, D. Elucidation of the Collision Induced Dissociation Pathways of Water and Alcohol Coordinated Complexes Containing the Uranyl Ion. *J. Am. Soc. Mass Spectrom.* **2003,** *14,* 1205–1214.
19. Chien, W.; Anbalagan, V.; Zandler, M.; Van Stipdonk, M. J. Intrinsic Hydration of Monopositive Uranyl Hydroxide, Nitrate, and Acetate Cations. *J. Am. Soc. Mass Spectrom.* **2004,** *15,* 777–783.
20. Van Stipdonk, M. J.; Chien, W.; Anbalagan, V.; Gresham, G.; Groenewold, G. Oxidation of 2-Propanol Ligands during Collision-Induced Dissociation of a Gas-Phase Uranyl Complex. *Int. J. Mass Spectrom.* **2004,** *237,* 175–183.
21. Van Stipdonk, M. J.; Chien, W.; Anbalagan, V.; Bulleigh, K.; Hanna, D.; Groenewold, G. Gas-Phase Complexes Containing the Uranyl Ion and Acetone. *J. Phys. Chem. A* **2004,** *108,* 10448–10457.
22. Jiao, C. Q.; Ranatunga, D. R. A.; Vaugn, W. E.; Freiser, B. S. A Pulsed-Leak Valve for Use with Ion Trapping Mass Spectrometers. *J. Am. Soc. Mass Spectrom.* **1996,** *7,* 118–122.
23. Campbell, S.; Rodgers, M. T.; Marzluff, E. M.; Beauchamp, J. L. Deuterium Exchange Reactions as a Probe of Biomolecule Structure. Fundamental Studies of Gas Phase H/D Exchange Reactions of Protonated Glycine Oligomers with D_2O, CD_3OD, CD_3CO_2D, and ND_3. *J. Am. Chem. Soc.* **1995,** *117,* 12840–12854.
24. Bartmess, J. E.; Georgiadis, R. M. Empirical Methods for Determination of Ionization Gauge Relative Sensitivities for Different Gases. *Vacuum* **1983,** *33,* 149–153.
25. Anderson, U. N.; Bojesen, G. Gas-Phase Ion/Molecule Reactions of Doubly Charged Clusters of Fe^{2+} or Mn^{2+} and Methanol with Ammonia. *Int. J. Mass Spectrom. Ion Processes* **1996,** *153,* 1–7.
26. Reid, G. E.; O'Hair, R. A. J.; Styles, M. L.; McFayden, W. D.; Simpson, R. J. Gas Phase Ion-Molecule Reactions in a Modified Ion Trap: H/D Exchange of Noncovalent Complexes and Coordinatively Unsaturated Platinum Complexes. *Rapid Commun. Mass Spectrom.* **1998,** *12,* 1701–1708.
27. Nielsen, S. B.; Bojesen, G. Ligand and H/D Exchange of $Mn(H_2O)_6^{2+}$ and $Cu(OH)(H_2O)_4^+$ in the Gas Phase. *Chem. Commun.* **1998**, 613–614.
28. Molina-Svendsen, H.; Bojesen, G.; McKenzie, C. J. Gas-Phase Reactivity of Coordinatively Unsaturated Transition Metal Complex Ions Toward Molecular Oxygen. *Inorg. Chem.* **1998,** *37,* 1981–1983.
29. Vachet, R. W.; Hartman, J. A. R.; Callahan, J. H. Ion-Molecule Reactions in a Quadrupole Ion Trap as a Probe of the Gas-Phase Structure of Metal Complexes. *J. Mass Spectrom.* **1998,** *33,* 1209–1225.
30. Vachet, R. W.; Callahan, J. H. Quadrupole Ion Trap Studies of the Structure and Reactivity of Transition Metal Ion Pair Complexes. *J. Mass Spectrom.* **2000,** *35,* 311–320.
31. Vachet, R. W.; Hartman, J. R.; Gertner, J. W.; Callahan, J. H. Investigation of Metal Complex Coordination Structure using Collision-Induced Dissociation and Ion-Molecule Reactions in a Quadrupole Ion Trap Mass Spectrometer. *Int. J. Mass Spectrom.* **2001,** *204,* 101–112.
32. Combariza, M. Y. Gas-Phase Ion-Molecule Reactions of Transition Metal Complexes: The Effect of Different Coordination Spheres on Complex Reactivity. *J. Am. Soc. Mass Spectrom.* **2002,** *13,* 813–825.
33. Combariza, M. Y.; Vachet, R. W. The Utility of Ion-Molecule Reactions in a Quadrupole Ion Trap Mass Spectrometer for Analyzing Metal Complex Coordination Structure. *Anal. Chim. Acta* **2003,** *496,* 233–248.
34. Combariza, M. Y.; Fermann, J. T.; Vachet, R. W. Are Gas-Phase Reactions of Five-Coordinate Divalent Metal Ion Complexes Affected by Coordination Geometry? *Inorg. Chem.* **2004,** *43,* 2745–2753.

35. Jennings, K. R.; Kemp, T. J.; Read, P. A. Cluster Formation in the Fast Atom Bombardment (FAB) Mass Spectra of Dioxouranium(VI) Dinitrate and Diacetate. *Inorg. Chim. Acta* **1989,** *157,* 157–159.
36. Kemp, T. J.; Jennings, K. R.; Read, P. A. Formation and Decomposition of Uranium-Oxygen Clusters in Fast Atom Bombardment of Dioxouranium(VI) Salts. *J. Chem. Soc. Dalton Trans.* **1995,** *1995,* 885–889.
37. Pospieszna-Markiewicz, I.; Radecka-Paryzek, W. The New Macrocyclic and Acyclic Complexes of the Uranyl Ion: Uranyl-Oxygen Cluster Formation in Fast Atom Bombardment Mass Spectra. *J. Alloys Compd.* **2004,** *374,* 253–257.
38. Brown, D. A.; Ismail, S. Synthesis of Dioxouranium Dialkylhydromates: Cluster Formation in Fast Atom Bombardment Mass Spectra (FAB-MS). *Inorg. Chim. Acta* **1990,** *171,* 42–43.
39. Formosinho, S. J.; Burrows, H. D.; da Graca-Miguel, M.; Azenha, M. E. D. G.; Saraiva, I. M.; Ribeiro, A. C. D. N.; Khudyakov, I. V.; Gasanov, R. G.; Bolte, M.; Sarakha, M. Deactivation Processes of the Lowest Excited State of $[UO_2(H_2O)_5]^{2+}$ in Aqueous Solution. *Photochem. Photobiol. Sci.* **2003,** *2,* 569–575.
40. Henis, J. M. S. An Ion Cyclotron Resonance Study of Ion-Molecule Reactions in Methanol. *J. Am. Chem. Soc.* **1968,** *90,* 844–851.
41. Kleingeld, J. C.; Nibbering, N. M. M. A Fourier Transform Ion Cyclotron Resonance Study of the Mechanism of Formation of Protonated Dimethyl Ether from Methanol by Use of Naturally Occurring ^{18}O. *Org. Mass Spectrom.* **1982,** *17,* 136–139.
42. Mollah, S.; Pris, A. D.; Johnson, S. K.; Gwizdala, A. B.; Houk, R. S. Identification of Metal Cations, Metal Complexes, and Anions by Electrospray Mass Spectrometry in the Negative Ion Mode. *Anal. Chem.* **2000,** *72,* 985–991.
43. Li, F.; Byers, M. A.; Houk, R. S. Tandem Mass Spectrometry of Metal Nitrate Negative Ions Produced by Electrospray Ionization. *J. Am. Soc. Mass Spectrom.* **2003,** *14,* 671–679.
44. Kaplan, L.; Hildebrandt, R. A.; Ader, M. The Trinitrouranyl Ion in Organic Solvents. *J. Inorg. Nucl. Chem.* **1956,** *2,* 153–163.
45. Barclay, G. A.; Sabine, T. M.; Taylor, J. C. The Crystal Structure of Rubidium Uranyl Nitrate: A Neutron Diffraction Study. *Acta Crystallogr.* **1965,** *19,* 205–209.